Editors' Suggestion | Featured in Physics

Measuring the Electrical Resistivity of Liquid Iron to 1.4 Mbar

Kenji Ohta,[1,*] Sho Suehiro,[1] Saori I. Kawaguchi,[2] Yoshiyuki Okuda,[1,3] Tatsuya Wakamatsu,[1] Kei Hirose,[3,4] Yasuo Ohishi,[2] Manabu Kodama,[5] Shuichiro Hirai,[5] and Shintaro Azuma[1]

[1]*Department of Earth and Planetary Sciences, Tokyo Institute of Technology, Tokyo 152-8551, Japan*
[2]*Japan Synchrotron Radiation Research Institute, SPring-8, Hyogo 679-5198, Japan*
[3]*Department of Earth and Planetary Science, The University of Tokyo, Tokyo 113-0033, Japan*
[4]*Earth-Life Science Institute, Tokyo Institute of Technology, Tokyo 152-8550, Japan*
[5]*Department of Mechanical Engineering, Tokyo Institute of Technology, Tokyo 152-8551, Japan*

(Received 24 November 2022; accepted 4 May 2023; published 26 June 2023)

We determined the electrical resistivity of liquid Fe to 135 GPa and 6680 K using a four-probe method in a diamond-anvil cell combined with two novel techniques: (i) enclosing a molten Fe in a sapphire capsule, and (ii) millisecond time-resolved simultaneous measurements of the resistance, x-ray diffraction, and temperature of instantaneously melted Fe. Our results show the minimal temperature dependence of the resistivity of liquid Fe and its anomalous resistivity decrease around 50 GPa, likely associated with a gradual magnetic transition, both in agreement with previous *ab initio* calculations.

DOI: 10.1103/PhysRevLett.130.266301

Introduction.—The physical properties of iron (Fe) under various pressure-temperature ($P-T$) conditions are interesting to study because of its geoscientific importance, various polymorphisms, and its puzzling electronic and magnetic behavior (e.g., [1–4]). Dense liquid Fe holds rich predictions regarding its electrical and magnetic properties. A semitheoretical deduction proposed a constant electrical resistivity (ρ) (the reciprocal of electrical conductivity) of Fe of about 120 $\mu\Omega\,\mathrm{cm}$ along its melting curve, resulting in the low electrical and thermal conductivities of the Earth's outer core composed of liquid Fe alloy [5,6]. Subsequent to these legendary works, *ab initio* electron-phonon scattering calculations based on density functional theory (DFT) [7,8] showed that the electrical resistivity of liquid Fe under the Earth's outer core pressures (136–330 GPa) is much lower than previously thought [5,6], which accelerated the reconsideration of the high $P-T$ transport properties of Fe (and its alloys) and the Earth's thermal history (e.g., [9,10]). As is the case for many metals, including Fe, the temperature dependence of the resistivity of the molten metal is smaller than that of the solid phase(s) (Fig. S1 [11]), which may also be true even at a pressure of 136 GPa [7]. Electron-electron scattering in liquid Fe, which was not considered in Refs. [7,8], is predicted to be negligible under core conditions based on the DFT plus dynamic mean field theory (DMFT) method applied to solid Fe phases [52], but estimates of the magnitude of the effect of electron-electron scattering in solid Fe vary among previous studies [52–54]. In addition, the paramagnetic to diamagnetic transition of liquid Fe is theoretically predicted to be accompanied by an anomalous decrease in the isothermal resistivity of liquid Fe in the range of 20–50 GPa [55].

The high $P-T$ experiment beyond the megabar pressure provides a critical test of the above theory-based predictions regarding the electrical properties of dense liquid Fe. However, experimental data on the electrical resistivity of liquid Fe at high pressures are sparse compared to those on solid phases. Because of the high fluidity and chemical reactivity of molten Fe, it has been difficult to conduct experiments in a high-pressure apparatus while maintaining the geometry and purity of the Fe sample. In 1989, Secco and Schloessin [56] first reported the resistivity of liquid Fe up to 7 GPa measured in a cubic anvil press (i.e., a large volume press). Similar experiments have collected more data up to 24 GPa, but with less consistency among them [57–61]. A laser-heated diamond-anvil cell (DAC) study showed the resistivity of liquid Fe at 26 and 51 GPa, but was subject to uncertainty due to possible changes in sample geometry during melting [62]. No shock compression experiments have measured the resistivity of liquid Fe. Therefore, to date, experimental data for the resistivity of liquid Fe up to 51 GPa and 2900 K [62] can be refered to, where the $P-T$ conditions and data accuracy are insufficient to verify the theory-based predictions mentioned above [5,7,8,52–55]. Technical improvements were needed to measure the electrical resistivity of molten metal at higher pressures.

In this Letter, we present the experimental determination of the electrical resistivity of liquid Fe up to 135 GPa and 6680 K, made possible by the introduction of two novel techniques combined with a four-probe resistance measurement in a DAC (Figs. S2 and S3 [11]). The first, which we call the sapphire capsule method, is the resistance measurement technique for a liquid Fe sample encapsulated by a sapphire single crystal in a DAC combined with a laser

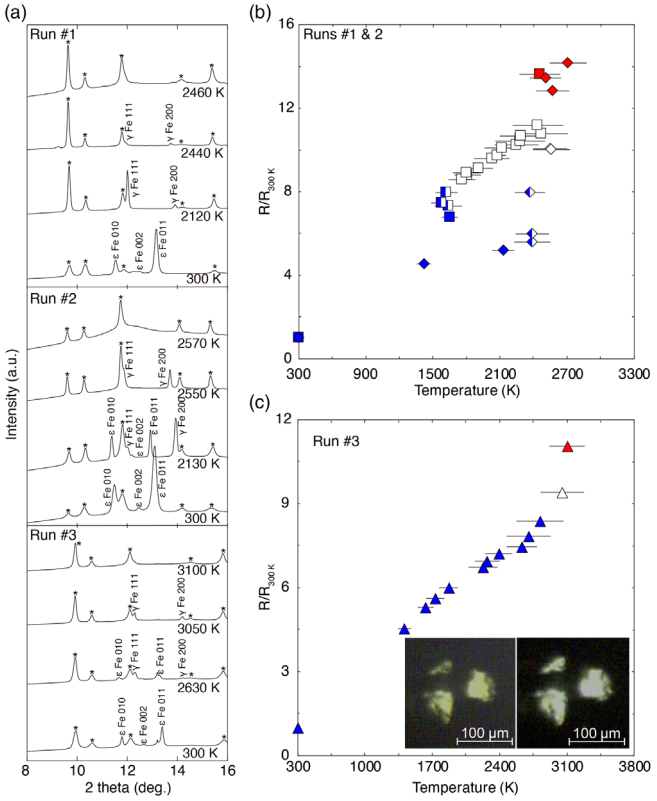

FIG. 1. Sapphire capsule method: (a) representative XRD patterns; (b),(c) electrical resistance normalized by the resistance at 300 K; and [(c) inset] photographs of the Fe sample taken through the diamond anvil before and after melting. Asterisks indicate sapphire diffraction peaks. Blue symbols, ε-Fe; open symbols, γ-Fe; half-filled symbols, mixture of ε and γ phases; red symbols, liquid Fe.

and internal resistance hybrid heating system (Fig. 1 and S4 of Ref. [11]). This technique aims to keep the geometry of the Fe sample unchanged during melting and to minimize a temperature gradient inside the sample. The latter, the instantaneous resistance detection method, simultaneously measures the electrical resistance, x-ray diffraction (XRD), and temperature of Fe instantaneously melted by a single high-power laser shot on a millisecond timescale (Fig. 2 and movie S1 in the Supplemental Material [11]), which aims to detect the liquid Fe resistance before the sample geometry changes. A total of nine separate runs using either of these methods were performed at BL10XU of SPring-8.

Results.—The sapphire capsule method was used in three separate runs conducted at approximately 40 and 70 GPa (Table S1 [11]). In run No. 1, we compressed the sapphire encapsulated Fe sample to 44 GPa at 300 K and then performed simultaneous high $P-T$ resistance and XRD measurements to melting conditions (Fig. S5 [11]). The XRD peaks of ε-Fe and sapphire were observed at 300 K, and the transitions from ε to γ and from γ to liquid were confirmed during heating [Fig. 1(a)]. The measured resistance showed a jump over melting, as repeatedly shown in previous studies (e.g., [56]). At the melting temperature of 2460 K at about 40 GPa, the resistance jump across melting was 21.7% [Fig. 1(b)]. We then performed another run (run No. 2) at an initial pressure of 44 GPa to confirm the reproducibility of the first run. We again observed the phase transition sequences and the corresponding resistance jump same as in run No. 1, and were able to obtain the diffuse scattering signal from the liquid, demonstrating sample melting [Figs. 1(a) and 1(b)]. The temperature response of the resistance in the second run was slightly different from that in run #1 in a temperature range between 2100 and 2400 K, which is due to a sluggish phase transition from ε to γ depending on the pace of temperature increase [63] (Table S1 [11]). The third set of experiments (run No. 3) was performed around 70 GPa. Similarly, we observed the jump in resistance when the XRD peaks of γ-Fe disappeared [Fig. 1(c)].

After temperature quenching, the sample resistance showed the same value as before heating, and no additional XRD peaks other than those of Fe and sapphire were detected. Importantly, we did not find any change in the sample geometry after melting under a microscope [Fig. 1(c) insets]. Furthermore, the melting temperatures found in the present experiments are consistent with a melting curve of Fe [64] (Fig. S5 [11]). These facts guarantee no change in sample geometry during melting and no chemical contamination from the surroundings (sapphire and diamond anvils) during the heating experiment, hence the reliability of the obtained resistivity of pure liquid Fe. Although we attempted to recover the sample to ambient conditions, the sapphire capsule is hard but brittle, so the capsule and the Fe sample were smashed up.

The instantaneous resistance detection method was used to perform six separate runs over a pressure range of 42 to 135 GPa (Table S2 [11]). The core of this method is high-speed, simultaneous measurements of XRD in 1 ms, sample resistance in 2.25 ms, and temperature in 10 ms. During the synchronized data acquisition, the Fe sample was melted by a double-sided laser heating for a short period of time, about 1–6 s (movie S1 [11]). The short-time laser heating allowed us to reach temperatures well above the melting temperature of Fe (Fig. S5 [11]).

Figure 2 shows representative experimental data for which we started heating at 61 GPa (run No. 4). The high-power laser shot heating began approximately 1.102 s after the start of the synchronized data acquisition ($t=0$ in Fig. 2) and continued for approximately 3 s, resulting in a $P-T$ condition of 105 GPa and 5200 K at $t=1.125$ s, much higher than the melting point of Fe [Fig. 2(a) and S5 [11]]. No XRD peaks of solid Fe were observed at $t=1.125$ s, indicating melting (Fig. S6 [11]). The measured resistance responded to sudden temperature changes by turning the laser beam on and off; a jump in resistance at the beginning of heating ($t>1.102$ s), a gradual increase during melting ($t>1.125$ s), and a slight drop followed by

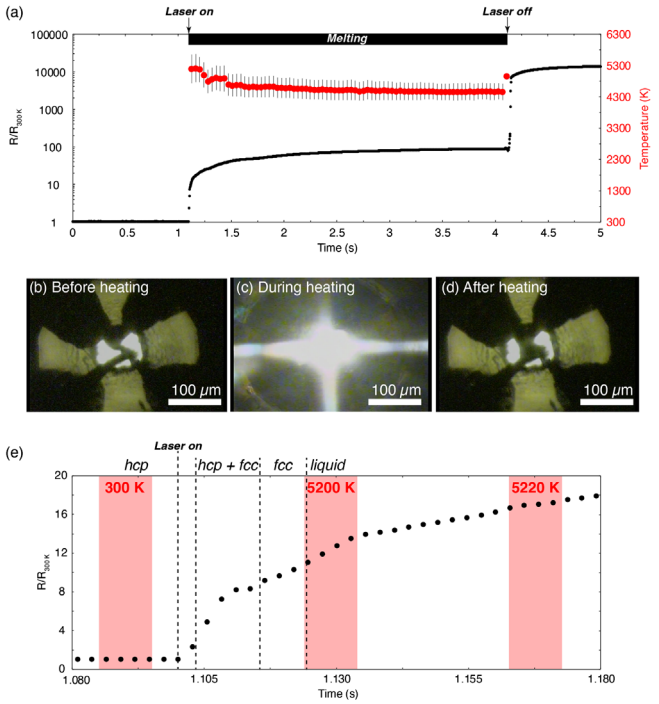

FIG. 2. Instantaneous resistance detection method: (a) Representative time (t) series of temperature and resistance (normalized by room-T resistance at $t = 0.000$) data obtained in run No. 4, in which the maximum $P-T$ condition was 107 GPa and 5200 K. (b)–(d) Photomicrographs of a sample chamber viewed through a diamond anvil before, during, and after laser heating. (e) Close-up view of (a) in $t = 1.080$–1.180 s. The Fe phase(s) at each time is identified from XRD measurements every 1 ms. Red rectangles indicate time windows of temperature measurements with 10 ms of exposure time.

a large jump when the laser was turned off ($t > 4.144$ s). The sample geometry obviously changed after the laser heating for about 3 s [Figs. 2(b)–2(d)], and Fig. S7 [11]]. In fact, after temperature quenching, the sample resistance did not return to its preheating value, which should be the result of sample deformation and possible chemical reaction during melting.

Figure 2(e) is a close-up of Fig. 2(a) in a time range from $t = 1.080$ to 1.180 s. We confirmed the Fe melting by the disappearance of the XRD peaks of Fe at $t = 1.125$ s (Fig. S6 [11]), and obtained its resistance at the same time. We took this resistance datum as the resistance of liquid Fe at 105 GPa and 5200 K, considering that the sample deformation and chemical reaction had not yet occurred at this time (Supplemental Material [11]). The data after $t = 1.125$ s are not used because of possible changes in sample geometry and chemical reactions. Other runs (runs No. 5–No. 9) showed the different time evolution of the measured resistance, which can be attributed to the extent and timing of the sample deformation and reaction (Fig. S8 [11]). As in run No. 4, we obtained the electrical resistance of liquid Fe at a time within 1 ms immediately after melting at 42, 49, 65, 79, and 135 GPa (Table S2 [11]).

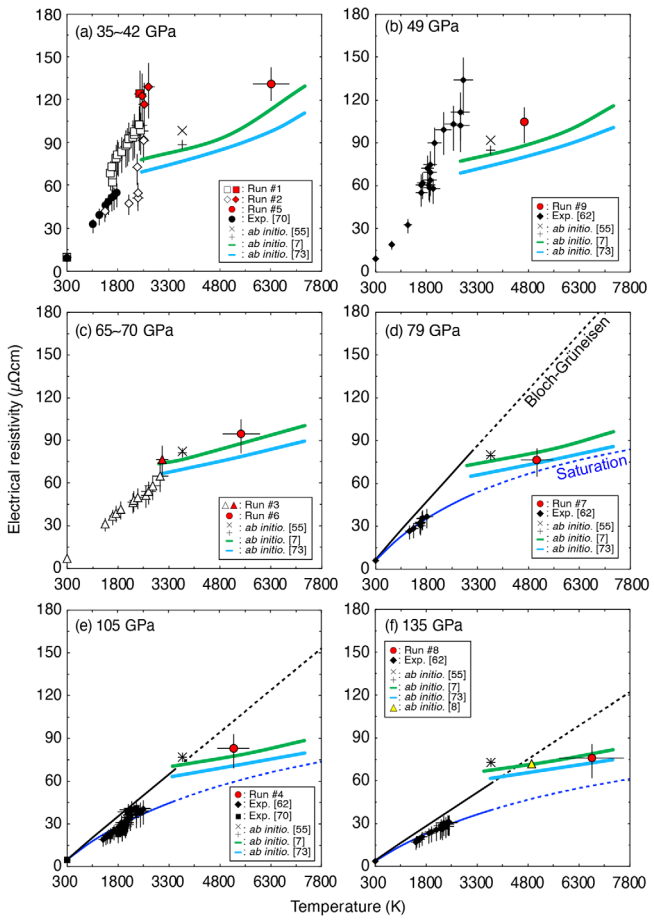

FIG. 3. Temperature dependence of the resistivity of Fe at (a) ~40 GPa (runs No. 1, No. 2, and No. 5), (b) ~49 GPa (run No. 9), (c) ~70 GPa (runs No. 3 and No. 6), (d) ~79 GPa (run No. 7), (e) ~105 GPa (run No. 4), and (f) ~135 GPa (run No. 8). Red and white symbols represent the present data for the resistivity of liquid and solid Fe, respectively. Black diamonds, circles, and squares are our previously reported resistivities of Fe [62,70]. Black and blue lines indicate the resistivities of ε-Fe predicted by the Bloch-Grüneisen formula and the resistivity saturation model [Eq. (1)], respectively [62]. The green and light blue lines and the yellow triangle show the resistivity of liquid Fe based on *ab initio* calculations [7,8,73]. Plus, and cross symbols indicate the liquid Fe resistivities calculated from spin-polarized the Perdew-Burke-Ernzerhof (PBE) formulation and spin-degenerated PBE, respectively [55]. To calculate the pressures at which the computations are performed as a function of density, we used an EOS of liquid Fe [74].

The electrical resistivity of liquid Fe at high pressures.— The obtained resistance data for liquid Fe are converted to its high $P-T$ resistivity (Fig. 3). Our experiments provide the experimentally constrained resistivity of liquid Fe to more than two times higher pressures than in previous experiments [56,57,59–62,65,66]. We confirmed that the temperature dependence of the resistivity of liquid Fe is smaller than that of solids at about 40 and 70 GPa [Figs. 3(a) and 3(c)]. de Koker *et al.* [7] showed that the

resistivity of liquid Fe does not follow the resistivity extrapolated by the Bloch-Grüneisen formula for solid Fe, and the present results observed the similar behavior. We previously observed thermally driven "resistivity saturation" in ε-Fe up to 157 GPa [62] [Figs. 3(d)–3(f)]; the resistivity of the metal asymptotically approaches the "saturation" resistivity (ρ_{sat}) with increasing temperature [67,68]. For pure solid metals, the temperature dependence of the electrical resistivity, including the resistivity saturation effect, is expressed empirically by the shunt resistor model [69]:

$$\frac{1}{\rho_{\mathrm{tot}}} = \frac{1}{\rho_{\mathrm{BG}}} + \frac{1}{\rho_{\mathrm{sat}}}, \tag{1}$$

where ρ_{tot} is the total electrical resistivity, and ρ_{BG} is the resistivity calculated from the Bloch-Grüneisen formula. Saturation is also observed in liquid metals, and ρ_{sat} may be slightly higher than in solids because of the reduction of the mean free path of electrons due to melting. In previous experiments, the resistivities of liquid Fe were found to be 10%–35% higher than those of solid Fe [62,70], which is a natural consequence of the loss of long-range order of atomic coordination due to melting, resulting in a shorter mean free path of electrons [Figs. 3(b) and 3(d)–3(f)]. We directly determined the magnitude of a resistance jump across melting at about 40 and 70 GPa to be 22%–28% and 18%, respectively [Figs. 1(a) and 1(c)]. According to previous theoretical calculations [71,72], the resistivity contrast across the ε-liquid boundary was predicted to gradually decrease by about 10% with increasing pressure towards 330 GPa, the pressure of the Earth's inner core boundary.

The resistivity of liquid Fe obtained at 135 GPa and 6680 K agrees well with estimates based on *ab initio* calculations [7,8,55,73], as do other present results above 70 GPa [Figs. 3(c)–3(f)]. These theoretical studies calculated only electron-phonon scattering, while different scattering mechanisms (interactions of electron-phonon, electron-magnon, electron-electron, and electron-lattice defects) should have contributed more or less to the present experimental data. Therefore, the fact that our experimental results are in agreement with these calculations indicates that the effect of electron-phonon scattering is still dominant under the present experimental $P-T$ conditions. Pourovskii *et al.* [52] applied the DFT and DMFT calculations to Fe and concluded that thermal disorder suppresses the non-Fermi-liquid behavior of α-Fe, which reduces the electron-electron scattering at high temperatures, which is likely to be the case for liquid Fe as well.

We estimated the resistivity of liquid Fe along its melting curve from the present data and the temperature dependence of the resistivity of liquid Fe proposed by de Koker *et al.* [7] (Fig. 4 and Table S3 of [11]), showing that the resistivity of liquid Fe at the melting point decreases from 1 bar to about 5 GPa (corresponding to the triple point of $\delta-\gamma$–liquid), remains almost constant at 120 μΩ cm up to 40 GPa, and then shifts to a value as low as the theoretical calculations of about 70 μΩ cm [7,8,55,73]. Stacey and Anderson [5] previously estimated the electrical resistivity of the Earth's core by assuming that the resistivity of liquid Fe is constant along its melting curve. This assumption is only valid in a pressure range from 5 to about 40 GPa, and therefore they overestimated the resistivity in the core pressure range (>136 GPa). For Mars and smaller terrestrial bodies in our solar system, the resistivity of liquid pure Fe at their core conditions is about 120 μΩ cm, which is the lower limit of the core resistivity (note that the cores should contain some impurity elements that increase the resistivity). On the other hand, for the Earth, and probably Venus if its core is liquid [75], the lower limit of their liquid core resistivity is about 80 μΩ cm (Fig. 4). Such a nonlinear pressure dependence of the resistivity of liquid Fe, as revealed by experiments, must be taken into account in the estimates of the conductivity of planetary metallic cores.

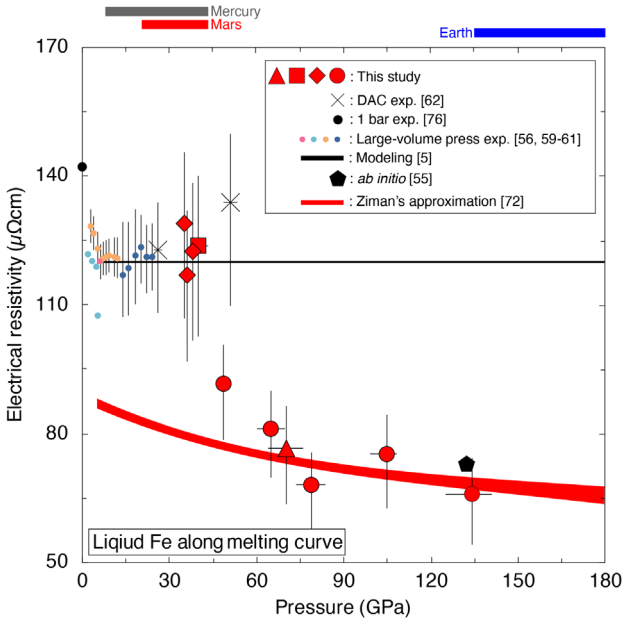

FIG. 4. The resistivity of liquid Fe along the melting curve. Red symbols indicate the resistivity of liquid Fe determined in this study. Our data (red circles) were calculated from the measured values and the temperature dependence of the liquid Fe resistivity proposed by Ref. [7] [Figs. 3(b)–3(f)]. The resistivity of liquid Fe at 1 bar is shown as a black circle [76]. Smaller circles show the experimentally determined resistivities of liquid Fe in large volume presses (light blue, [56]; orange, [59]; pink, [60]; navy, [61]). Crosses are the resistivities of liquid Fe from our previous study [62]. Pentagon symbol indicates the liquid Fe resistivities calculated from the spin-polarized PBE [55]. The black line shows the invariant resistivity predicted by Ref. [5]. The red curve is based on Ziman's approximation [72]. The bars at the top of the figure show the pressure ranges of the cores of the Earth, Mars, and Mercury [77,78].

The lack of agreement between experiment and theory on the resistivity of liquid Fe at low pressures (even 1 bar) has been a long-standing problem. Indeed, the present results do not agree with the results of *ab initio* calculations at low pressures below 49 GPa, but become more harmonic with increasing pressure (Fig. 3). Korell *et al.* [55] investigated the effect of magnetism on the electronic state of liquid Fe by spin-polarized DFT-based simulations using the Kubo-Greenwood equation and showed that spin polarization must be taken into account at relatively low pressures, in order to reconcile *ab initio* calculations with experiments. In addition, they [55] showed the gradual magnetic transition between 20 and 50 GPa along the 3700 K isotherm, which is accompanied by a decrease in the resistivity. The decrease in the liquid Fe resistivity observed in this study between ~40 and ~70 GPa could be a consequence of the magnetic transition in liquid Fe as predicted by Korell *et al.* [55] (Fig. 4).

We thank Dr. Kobayashi and Dr. Hasegawa for their technical assistance. The synchrotron x-ray diffraction experiments were performed at the BL10XU of SPring-8 (Proposal No. 2017–2021A, B0072). This report is based on work supported by the JSPS KAKENHI Grants No. 19J13936 (S. S.), and No. 19H00716 (K. O.). All data supporting the results of this study are available from the corresponding author upon reasonable request.

*k-ohta@geo.titech.ac.jp

[1] S. Tateno, K. Hirose, Y. Ohishi, and Y. Tatsumi, Science **330**, 359 (2010).
[2] A. B. Belonoshko, T. Lukinov, J. Fu, J. Zhao, S. Davis, and S. I. Simak, Nat. Geosci. **10**, 312 (2017).
[3] K. Shimizu, T. Kimura, S. Furomoto, K. Takeda, K. Kontani, Y. Onuki, and K. Amaya, Nature (London) **412**, 316 (2001).
[4] B. W. Lebert *et al.*, Proc. Natl. Acad. Sci. U.S.A. **116**, 20280 (2019).
[5] F. D. Stacey and O. L. Anderson, Phys. Earth Planet. Inter. **124**, 153 (2001).
[6] F. D. Stacey and D. E. Loper, Phys. Earth Planet. Inter. **161**, 13 (2007).
[7] N. de Koker, G. Steinle-Neumann, and V. Vlcek, Proc. Natl. Acad. Sci. U.S.A. **109**, 4070 (2012).
[8] M. Pozzo, C. Davies, D. Gubbins, and D. Alfe, Nature (London) **485**, 355 (2012).
[9] K. Ohta and K. Hirose, Nat. Sci. Rev. **8**, nwaa303 (2020).
[10] Q. Williams, Annu. Rev. Earth Planet Sci. **46**, 47 (2018).
[11] See Supplemental Material at http://link.aps.org/supplemental/10.1103/PhysRevLett.130.266301 for experimental details and a description of the performed FEM simulations, which includes Refs. [12–51].
[12] H. Gomi and K. Hirose, Phys. Earth Planet. Inter. **247**, 2 (2015).
[13] H. Gomi, K. Hirose, H. Akai, and Y. Fei, Earth Planet. Sci. Lett. **451**, 51 (2016).
[14] H. Inoue, S. Suehiro, K. Ohta, K. Hirose, and Y. Ohishi, Earth Planet. Sci. Lett. **543**, 116357 (2020).
[15] D. Jaccard, A. T. Holmes, G. Behr, Y. Inada, and Y. Onuki, Phys. Lett. A **299**, 282 (2002).
[16] K. Ohta, S. Suehiro, K. Hirose, and Y. Ohishi, C. R. Geoscience **351**, 147 (2019).
[17] C. T. Seagle, E. Cottrell, Y. Fei, D. R. Hummer, and V. B. Prakapenka, Geophys. Res. Lett. **40**, 5377 (2013).
[18] S. Suehiro, K. Ohta, K. Hirose, G. Morard, and Y. Ohishi, Geophys. Res. Lett. **44**, 8254 (2017).
[19] C. Zhang, J.-F. Lin, Y. Liu, S. Feng, C. Jin, M. Hou, and T. Yoshino, J. Geophys. Res. **123**, 3564 (2018).
[20] Y. Zhang, M. Hou, P. Driscoll, N. P. Salke, J. Liu, E. Greenberg, V. B. Prakapenka, and J.-F. Lin, Earth Planet. Sci. Lett. **553**, 116614 (2021).
[21] Y. Zhang, M. Hou, G. Liu, C. Zhang, V. B. Prakapenka, E. Greenberg, Y. Fei, R. E. Cohen, and J.-F. Lin, Phys. Rev. Lett. **125**, 078501 (2020).
[22] N. Hirao, S. I. Kawaguchi, K. Hirose, K. Shimizu, E. Ohtani, and Y. Ohishi, Matter Radiat. Extremes **5**, 018403 (2020).
[23] S. I. Kawaguchi, Y. Nakajima, K. Hirose, T. Komabayashi, H. Ozawa, S. Tateno, Y. Kuwayama, S. Tsutsui, and A. Q. R. Baron, J. Geophys. Res. **122**, 3624 (2017).
[24] Y. Nakajima, S. Imada, K. Hirose, T. Komabayashi, H. Ozawa, S. Tateno, S. Tsutsui, Y. Kuwayama, and A. Q. Baron, Nat. Commun. **6**, 8942 (2015).
[25] G. Aquilanti, A. Trapananti, A. Karandikar, I. Kantor, C. Marini, O. Mathon, S. Pascarelli, and R. Boehler, Proc. Natl. Acad. Sci. U.S.A. **112**, 12042 (2015).
[26] R. Sinmyo, K. Hirose, and Y. Ohishi, Earth Planet. Sci. Lett. **510**, 45 (2019).
[27] A. Dewaele, P. Loubeyre, F. Occelli, M. Mezouar, P. I. Dorogokupets, and M. Torrent, Phys. Rev. Lett. **97**, 215504 (2006).
[28] L. S. Dubrovinsky, S. K. Saxena, and P. Lazor, Phys. Chem. Miner. **25**, 434 (1998).
[29] N. Tsujino, Y. Nishihara, Y. Nakajima, E. Takahashi, K.-i. Funakoshi, and Y. Higo, Earth Planet. Sci. Lett. **375**, 244 (2013).
[30] R. A. Secco, Phys. Earth Planet. Inter. **265**, 23 (2017).
[31] M. A. Tupta, KEITHLEY, 2007, https://www.tek.com/en/documents/technical-article/ac-versus-dc-measurement-methods-low-power-nanotech-and-other-sensitive-d.
[32] D. Pennicard *et al.*, J. Instrum. **13**, C01026 (2018).
[33] S. Tateno, T. Komabayashi, K. Hirose, N. Hirao, and Y. Ohishi, Am. Mineral. **104**, 718 (2019).
[34] J. G. Hust and A. B. Lankford, in *Standard Reference Materials* (National Bureau of Standards of Standards, 1984), https://www.nist.gov/system/files/documents/2016/10/06/SP260-90.PDF.
[35] P. W. Bridgman, Proc. Am. Acad. Arts Sci. **81**, 167 (1952).
[36] H. Ohno, J. Phys. Soc. Jpn. **31**, 92 (1971).
[37] X. Sha and R. E. Cohen, J. Phys. Condens. Matter **23**, 075401 (2011).
[38] S. S. Lobanov and Z. M. Geballe, Geophys. Res. Lett. **49**, e2022GL100379 (2022).
[39] M. Kodama, S. Komiyama, A. Ohashi, N. Horikawa, K. Kawamura, and S. Hirai, J. Power Sources **462**, 228160 (2020).

[40] A. M. Hofmeister, Phys. Chem. Miner. **41**, 361 (2014).
[41] D. S. Smith, S. Fayette, S. Grandjean, and C. Martin, J. Am. Ceram. Soc. **86**, 105 (2003).
[42] A. M. Hofmeister, A. Sehlke, G. Avard, A. J. Bollasina, G. Robert, and A. G. Whittington, J. Volcanol. Geotherm. Res. **327**, 330 (2016).
[43] Y. Kono, C. Kenney-Benson, Y. Shibazaki, C. Park, G. Shen, and Y. Wang, Phys. Earth Planet. Inter. **241**, 57 (2015).
[44] S. Merkel, H. P. Liermann, L. Miyagi, and H. R. Wenk, Acta Mater. **61**, 5144 (2013).
[45] M. Yousuf, P. C. Sahu, and K. G. Rajan, Phys. Rev. B **34**, 8086 (1986).
[46] J. B. Van Zytveld, J. Phys. (Paris), Colloq. **41**, C8 (1980).
[47] M. Beutl, G. Pottlacher, and H. Jager, Int. J. Thermophys. **15**, 1323 (1994).
[48] R. A. Matula, J. Phys. Chem. Ref. Data **8**, 1147 (1979).
[49] J. W. Arblaster, Johnson Matthey Technol. Rev. **59**, 174 (2015).
[50] J. W. Arblaster, Johnson Matthey Technol. Rev. **60**, 4 (2016).
[51] Z. Wang, H. Mao, and S. K. Saxena, J. Alloys Compd. **299**, 287 (2000).
[52] L. V. Pourovskii, J. Mravlje, M. Pozzo, and D. Alfe, Nat. Commun. **11**, 4105 (2020).
[53] J. Xu, P. Zhang, K. Haule, J. Minar, S. Wimmer, H. Ebert, and R. E. Cohen, Phys. Rev. Lett. **121**, 096601 (2018).
[54] Y. Zhang *et al.*, Proc. Natl. Acad. Sci. U.S.A. **119**, e2119001119 (2022).
[55] J. A. Korell, M. French, G. Steinle-Neumann, and R. Redmer, Phys. Rev. Lett. **122**, 086601 (2019).
[56] R. A. Secco and H. H. Schloessin, J. Geophys. Res. **94**, 5887 (1989).
[57] I. C. Ezenwa and T. Yoshino, Icarus **360**, 114367 (2021).
[58] A. Pommier, Earth Planet. Sci. Lett. **496**, 37 (2018).
[59] R. E. Silber, R. A. Secco, W. Yong, and J. A. H. Littleton, Sci. Rep. **8**, 10758 (2018).
[60] Y. Yin, L. Wang, S. Zhai, and Y. Fei, J. Geophys. Res. **127**, e2021JE007116 (2022).
[61] W. Yong, R. A. Secco, J. A. H. Littleton, and R. E. Silber, Geophys. Res. Lett. **46**, 11065 (2019).
[62] K. Ohta, Y. Kuwayama, K. Hirose, K. Shimizu, and Y. Ohishi, Nature (London) **534**, 95 (2016).
[63] A. Kubo, E. Ito, T. Katsura, T. Shinmei, H. Yamada, O. Nishikawa, and M. Song, Geophys. Res. Lett. **30**, 1126 (2003).
[64] T. Komabayashi, J. Geophys. Res. **119**, 4164 (2014).
[65] I. C. Ezenwa and R. A. Secco, Crystals **9**, 359 (2019).
[66] I. C. Ezenwa and T. Yoshino, Rev. Sci. Instrum. **91**, 023903 (2020).
[67] H. Gomi, K. Ohta, K. Hirose, S. Labrosse, R. Caracas, M. J. Verstraete, and J. W. Hernlund, Phys. Earth Planet. Inter. **224**, 88 (2013).
[68] O. Gunnarsson, M. Calandra, and J. E. Han, Rev. Mod. Phys. **75**, 1085 (2003).
[69] H. Wiesmann, M. Gurvitch, H. Lutz, A. Ghosh, B. Schwarz, M. Strongin, P. B. Allen, and J. W. Halley, Phys. Rev. Lett. **38**, 782 (1977).
[70] S. Suehiro, T. Wakamatsu, K. Ohta, K. Hirose, and Y. Ohishi, High Press. Res. **39**, 579 (2019).
[71] M. Pozzo, C. Davies, D. Gubbins, and D. Alfè, Earth Planet. Sci. Lett. **393**, 159 (2014).
[72] F. Wagle and G. Steinle-Neumann, Geophys. J. Int. **213**, 237 (2018).
[73] F. Wagle, G. Steinle-Neumann, and N. de Koker, C. R. Geoscience **351**, 154 (2019).
[74] Y. Kuwayama, G. Morard, Y. Nakajima, K. Hirose, A. Q. R. Baron, S. I. Kawaguchi, T. Tsuchiya, D. Ishikawa, N. Hirao, and Y. Ohishi, Phys. Rev. Lett. **124**, 165701 (2020).
[75] J.-L. Margot, D. B. Campbell, J. D. Giorgini, J. S. Jao, L. G. Snedeker, F. D. Ghigo, and A. Bonsall, Nat. Astron. **5**, 676 (2021).
[76] R. S. Hixson, M. A. Winkler, and M. L. Hodgdon, Phys. Rev. B **42**, 6485 (1990).
[77] A. Rivoldini and T. Van Hoolst, Earth Planet. Sci. Lett. **377–378**, 62 (2013).
[78] S. C. Stähler *et al.*, Science **373**, 443 (2021).